Choose Your Subcarriers Wisely: Active Interference Cancellation for cognitive OFDM

Jorge F. Schmidt, *Member, IEEE,* Secundino Costas-Sanz and Roberto López-Valcarce, *Member, IEEE,*

Department of Signal Theory and Communications
University of Vigo, Spain

***Abstract*— A novel low complexity active interference cancellation (AIC) scheme for primary user (PU) protection is presented for application to cognitive OFDM systems, in which out-of-band radiation spilling over the PU protected band is to be minimized. A set of carefully selected cancellation subcarriers are modulated by appropriate linear combinations of the remaining data subcarriers. The combination weights are fixed so that, in contrast with previous AIC approaches, they need not be recomputed on a symbol-by-symbol basis. Weight optimization can thus be carried out offline, drastically reducing the online computational cost. In addition, it is shown that by carefully selecting the location of cancellation subcarriers, significant performance improvements can be achieved. Given that finding the optimal location is an intractable combinatorial problem, an heuristic approach is proposed, based on a greedy search which provides a good tradeoff. The proposed scheme is shown to outperform current AIC solutions both in terms of performance and computational cost, obtaining significant improvements in terms of notch depth, with almost 50 dB depth in typical settings, to protect a narrowband PU inside the secondary user OFDM band. Further, experimental measurements from the implementation of the proposed scheme on both professional and off-the-shelf hardware platforms validate its effectiveness.**

***Index Terms*— OFDM Cognitive Radio, Primary User Protection, Active Interference Cancellation, Low Complexity Design.**

I. Introduction

Orthogonal frequency division multiplexing (OFDM) has been widely adopted as the modulation technique for many broadband wireless communication systems because of its high spectrum efficiency and robustness against multipath fading. Further, its natural bandwidth partitioning makes it a particularly well suited modulation scheme for cognitive systems, where the transmit signal needs to be adjusted according to the available transmission spectrum. Nevertheless, the high out-of-band radiation (OBR) characteristic of OFDM remains a limiting factor for its application to cognitive systems, since it results in high interference for primary users (PUs) lying within the secondary user (SU) OFDM band. This interference is due to the high sidelobe levels of the Fast Fourier Transform (FFT) employed in standard OFDM. An intuitive approach to mitigate this FFT leakage over the PU band is to turn off, besides those subcarriers aligned with the PU, a number of additional data subcarriers adjacent to the protected band. However, OBR reduction improves slowly with the number of null subcarriers, and therefore this simple approach requires to sacrifice many data subcarriers, leading to a significant throughput loss.

Another approach for PU protection that has gained renewed interest in recent years replaces traditional OFDM modulation by a more sophisticated filter bank multicarrier (FBMC) scheme [1]. In FBMC, the spectral characteristic of the system subcarriers is improved to drastically reduce (at the cost of a higher complexity) the FFT leakage problem of traditional OFDM. While FBMC is a possible approach for PU protection in the near future, OFDM constitutes the multicarrier modulation scheme of choice in many communication standards already in use. This makes particularly important to develop PU protection schemes suitable for application in current OFDM-based standards. Therefore, the focus of this paper is on the OFDM PU protection problem.

Attention has been given to this problem in recent years, with several solutions reported in the literature. The use of multiple choice sequences and constellation expansion techniques were proposed in [2] and [3] respectively. Both techniques require the transmission of side information to the receiver and thus increase the system overhead. Other approaches such as active interference cancellation (AIC) schemes [4]-[8] and precoding techniques [9]-[13] do not require side information at the receiver, exhibiting good performance in terms of OBR reduction. Precoding techniques naturally lead to low complexity implementations at the transmitter, although the receiver needs to be aware of this fact and implement appropriate decoding of the received data. On the other hand, AIC schemes dedicate a subset of subcarriers (termed *cancellation subcarriers*) in order to reduce OBR, without altering the data subcarriers. This operation is completely transparent to the receiver, which just needs to discard cancellation subcarriers. Therefore an appealing property of AIC schemes is their straightforward implementation in current systems.

In AIC schemes, the cancellation subcarriers are modulated by some function (usually a linear combination) of the symbols transmitted in the data subcarriers. Most solutions in the litera-

Work supported by the Spanish Government, ERDF funds (TEC2010-21245-C02-02/TCM DYNACS, CONSOLIDER-INGENIO 2010 CSD2008-00010 COMONSENS), the Galician Regional Government (CN 2012/260 Atlant-TIC), and the Instituto de Investigaciones en Ingeniería Eléctrica (IIIE)-Consejo Nacional de Investigaciones Científicas y Técnicas (CONICET), Universidad Nacional del Sur, Argentina.

ture need to recompute the weights of the cancellation subcarriers at each OFDM symbol, making online computational cost a main concern [5]. This drawback is exacerbated by the need to impose additional constraints in the optimization problem in order to keep the power allocated to cancellation subcarriers at bay, as in the constrained Least Squares (LS) approach of [4]. Reduced-complexity LS formulations have been proposed in [7] and [8], but the resulting power allocated to cancellation subcarriers is not kept under control in the optimization process. In contrast, the low-complexity implementation in [6] imposes individual power constraints on each cancellation subcarrier, rather than a global constraint on the total power; with such approach, PU protection performance is significantly reduced as a consequence of having a smaller feasible set.

In view of the bottleneck that online computational cost represents for AIC schemes, it is not surprising that most research effort in the recent years has focused on trading off online complexity and performance. Comparatively, much less attention has been paid to the selection of the locations of cancellation subcarriers. Traditionally, these have been placed at the edges of the protected band, which may seem intuitive at first glance. However, there is no evidence of optimality for this choice, and in fact this arbitrary positioning sacrifices much of the flexibility of the AIC approach. Since the problem of optimizing the cancellation weights has the same complexity regardless of where the cancellation subcarriers are located, the choice of these locations yields additional degrees of freedom to the AIC design, which can be used to further enhance PU protection performance.

Nevertheless, exploiting these degrees of freedom is not straightforward: optimizing the location of the cancellation subcarriers is essentially a combinatorial problem and, given the large number of subcarriers used in current OFDM systems [14], [15], the number of possible assignments becomes extremely large. To the authors' knowledge, the only previous work in which an attempt is made to obtain an optimum assignment is [16], although the design goal is significantly different from the one considered here: in [16] it is assumed that channel state information (CSI) is available at the transmitter, and the goal is to maximize the system throughput subject to a mask constraint on the transmit power spectral density (PSD) as well as a total power constraint. In settings for which no CSI is available, it makes sense to focus on OBR reduction rather than throughput, as will be done in the sequel.

In this context, the contribution of this paper is twofold. First, for a given set of cancellation subcarriers, a novel optimization scheme for the AIC weights is derived. It can be implemented at low computational cost without sacrificing PU protection performance. Second, we propose a heuristic means to select the set of AIC subcarriers which yield good performance while avoiding an exhaustive search over all possible assignments. The benefits of adequately selecting the positions of the AIC subcarriers can be significant (several dB), and most importantly, they are obtained without involving any tradeoff with respect to the traditional allocation.

Regarding the weight optimization scheme, the proposed approach is based on the direct minimization of the radiated power spilling over the PU protected band, obtained as the integral of the PSD over such band. This method outperforms previous schemes which instead attempt to minimize the signal spectrum at a discrete set of frequencies within the PU band, and does away with the problem of deciding which specific frequencies to include in such set.

The result is a set of weights which is independent of the particular transmitted symbol, so that weight optimization can be performed offline. This also enables offline optimization of the set of AIC subcarriers. Therefore, the online computational cost incurred reduces to the computation of the linear combinations of the data using the pre-stored set of weights.

The remainder of this paper is organized as follows. The signal model is presented in Sec. II. Sec. III addresses the optimization of the cancellation weights and AIC subcarrier positions, whereas the computational complexity is analyzed in Sec. IV. The effectiveness of the proposed approach is validated in Sec. V, not only via simulations, but also with hardware implementations using realistic values of system parameters. Finally, conclusions are drawn in Sec. VI.

II. Signal Model

A cognitive SU OFDM transmission with N subcarriers and power equally distributed among data subcarriers is considered. Focus is made on the case where a narrowband PU signal lies within the considered SU transmission bandwidth[1]. It is assumed that the band $\mathcal{B}$ corresponding to the PU is covered by N_P contiguous SU subcarriers. SU subcarriers are allocated as follows: N_P subcarriers (aligned with band $\mathcal{B}$) plus N_C subcarriers are reserved for the OBR reduction task, whereas the remaining $N_D = N - N_P - N_C$ subcarriers are unaffected and used for data transmission.

Based on this subcarrier allocation, an $N \times N_D$ matrix $\boldsymbol{S}$ is defined, containing the N_D columns of the $N \times N$ identity matrix $\boldsymbol{I}_N$ corresponding to the set $\mathcal{D}$ of data subcarriers. Analogously, we define the $N \times (N_P + N_C)$ matrix $\boldsymbol{T}$ containing the columns of $\boldsymbol{I}_N$ corresponding to the set $\mathcal{C}$ of reserved subcarriers. Using these definitions, the $N \times 1$ vector modulating the SU subcarriers for a given OFDM symbol can be written as

$$\boldsymbol{x} = [\ x_0 \quad x_1 \quad \cdots \quad x_{N-1}\ ]^T = \alpha \boldsymbol{S}\boldsymbol{d} + \boldsymbol{T}\boldsymbol{c}, \qquad (1)$$

where $\boldsymbol{d}$ is the $N_D \times 1$ data vector, assumed zero-mean with covariance $E\{\boldsymbol{d}\boldsymbol{d}^H\} = \boldsymbol{I}_{N_D}$, and $\boldsymbol{c}$ is a $(N_P + N_C) \times 1$ vector containing the cancellation coefficients to be modulated on the reserved subcarriers. The scaling factor α, with $0 < \alpha \leq 1$, is a user-selected parameter that allows to allocate the available transmit power between the data and cancellation subcarriers, as will be seen in Sec. III. Also note that the SNR loss at the receiver is given by $10\log_{10}\alpha^2$ (dB) with respect to the case in which $\boldsymbol{x} = \boldsymbol{S}\boldsymbol{d}$ (for which no scaling is introduced and $\boldsymbol{c} = \boldsymbol{0}$, i.e., null subcarriers are used instead of active cancellation). Thus, the choice of α involves a tradeoff between OBR reduction at the transmitter and bit error rate at the receiver.

[1]The proposed approach can also target the reduction of adjacent channel interference in a straightforward manner.

To keep the presentation simple, conventional cyclic-prefix based OFDM is considered, in which a rectangular pulse shape is employed. Let Δ_f be the subcarrier spacing, and $T = (N + N_{\rm cp})T_{\rm s} = MT_{\rm s}$ the OFDM symbol duration, with $T_{\rm s} = 1/(N\Delta_f)$ and $M = N + N_{\rm cp}$ the length of the cyclic-prefix extended symbol, measured in samples. Following [17], the spectrum for each subcarrier, windowed over one OFDM symbol, is given by the main replica of the discrete-time Fourier transform (DTFT) of the length-M causal rectangular window employed. Such DTFT can be written as $W(\nu) = Me^{-j\pi M\nu}\,\mathrm{sinc}_M[\nu]$, where $\mathrm{sinc}_M[\cdot]$ stands for the periodic or aliased sinc function, defined as

$$\mathrm{sinc}_M[\nu] \triangleq \begin{cases} (-1)^{\nu(M-1)}, & \text{for } \nu \in \mathbb{Z}, \\ \frac{\sin(\pi M\nu)}{M\sin(\pi\nu)}, & \text{for } \nu \notin \mathbb{Z}, \end{cases} \tag{2}$$

and the linear phase term $e^{-j\pi M\nu}$ appears from considering a causal window. Particularizing $\nu = \frac{1}{N}\left(\frac{f}{\Delta_f} - k\right)$ to account for the OFDM structure, the spectrum corresponding to the k-th subcarrier for $k = 0, 1, \ldots, N-1$ is given by

$$\phi_k(f) = Me^{-j\pi\frac{M}{N}\left(\frac{f}{\Delta_f}-k\right)}\,\mathrm{sinc}_M\left[\frac{1}{N}\left(\frac{f}{\Delta_f} - k\right)\right]\mathcal{G}(f), \tag{3}$$

where $\mathcal{G}(f)$ denotes the frequency response of the interpolation filter used in the digital-to-analog (D/A) conversion step, and is assumed an ideal brickwall filter retaining only the spectrum replica within the system bandwidth. Using (3), the SU spectrum can be expressed as

$$X(f) = \sum_{k=0}^{N-1} x_k\phi_k(f) = \boldsymbol{x}^T\boldsymbol{\phi}(f), \tag{4}$$

where $\boldsymbol{\phi}(f) \triangleq [\ \phi_0(f)\quad \phi_1(f)\quad \cdots\quad \phi_{N-1}(f)\ ]^T$. From (1) and (4), the PU protection problem amounts to choosing the cancellation coefficients $\boldsymbol{c}$ (subject to appropriate design constraints) such that the resulting spectrum $X(f)$, measured over band $\mathcal{B}$, is 'small' in some sense. In the next section we address this problem by considering the radiated power over $\mathcal{B}$ as objective function.

III. PSD-based PU protection

A. Derivation of cancellation coefficients

We consider generating the cancellation coefficients $\boldsymbol{c}$ as linear combinations of the data symbols, i.e.,

$$\boldsymbol{c} = \boldsymbol{\Theta}\boldsymbol{d}, \tag{5}$$

where the $(N_P + N_C) \times N_D$ weight matrix $\boldsymbol{\Theta}$ is the parameter to be optimized. Note that $\boldsymbol{\Theta}$ is *fixed* and does not change from one OFDM symbol to the next (as long as the band $\mathcal{B}$ to protect does not change). Therefore, it can be computed offline, and thus the online complexity of the AIC scheme boils down to the computation of the product in (5) for each OFDM symbol.

Inserting (5) in (1) gives

$$\boldsymbol{x} = (\alpha\boldsymbol{S} + \boldsymbol{T}\boldsymbol{\Theta})\boldsymbol{d} = \boldsymbol{G}\boldsymbol{d}. \tag{6}$$

Since the operator $\boldsymbol{G} \triangleq \alpha\boldsymbol{S} + \boldsymbol{T}\boldsymbol{\Theta}$ is memoryless and static (time-invariant), the signal PSD can be approximated as

$$\begin{aligned} P_x(f) \approx E\left\{|X(f)|^2\right\} &= \boldsymbol{\phi}^H(f)E\{\boldsymbol{x}\boldsymbol{x}^H\}\boldsymbol{\phi}(f) \\ &= \boldsymbol{\phi}^H(f)\boldsymbol{G}E\{\boldsymbol{d}\boldsymbol{d}^H\}\boldsymbol{G}^H\boldsymbol{\phi}(f) \\ &= \mathrm{tr}\{\boldsymbol{G}^H\boldsymbol{\Phi}(f)\boldsymbol{G}\}, \end{aligned} \tag{7}$$

where we have introduced the Hermitian matrix $\boldsymbol{\Phi}(f) \triangleq \boldsymbol{\phi}(f)\boldsymbol{\phi}^H(f)$.

Let $P_{\max}$ be the available transmit power. Since our baseline is given by the case $\boldsymbol{x} = \boldsymbol{S}\boldsymbol{d}$ (i.e., $\alpha = 1$ and null subcarriers), we take $P_{\max}$ as the transmit power under those conditions:

$$P_{\max} = \int_{-\infty}^{\infty}\mathrm{tr}\{\boldsymbol{S}^T\boldsymbol{\Phi}(f)\boldsymbol{S}\}\mathrm{d}f. \tag{8}$$

The goal is to minimize the out-of-band radiation, under a constraint on the total transmit power, i.e.

$$\min_{\boldsymbol{\Theta}} \int_{\mathcal{B}} P_x(f)\mathrm{d}f \quad \text{s.t.} \int_{-\infty}^{\infty} P_x(f)\mathrm{d}f \le P_{\max}. \tag{9}$$

Let us introduce the $N \times N$ matrices

$$\boldsymbol{\Phi}_{\mathcal{B}} \triangleq \int_{\mathcal{B}}\boldsymbol{\Phi}(f)\mathrm{d}f, \qquad \boldsymbol{\Phi}_{\mathcal{T}} \triangleq \int_{-\infty}^{\infty}\boldsymbol{\Phi}(f)\mathrm{d}f, \tag{10}$$

so that (9) can be rewritten as

$$\begin{aligned} &\min_{\boldsymbol{\Theta}}\mathrm{tr}\{\boldsymbol{G}^H(\boldsymbol{\Theta})\boldsymbol{\Phi}_{\mathcal{B}}\boldsymbol{G}(\boldsymbol{\Theta})\} \\ &\text{s.t.}\quad \mathrm{tr}\{\boldsymbol{G}^H(\boldsymbol{\Theta})\boldsymbol{\Phi}_{\mathcal{T}}\boldsymbol{G}(\boldsymbol{\Theta})\} \le P_{\max}. \end{aligned} \tag{11}$$

Note from (8) and (10) that $P_{\max} = \mathrm{tr}\{\boldsymbol{S}^T\boldsymbol{\Phi}_{\mathcal{T}}\boldsymbol{S}\}$. As anticipated, since Problem (11) does not depend on any particular value of $\boldsymbol{d}$, it suffices to solve it offline and then store the optimal weights in memory. This is in contrast with previous AIC schemes, which need to compute a set of weights for each instance of the data vector $\boldsymbol{d}$.

In order to solve (11), consider first the *unconstrained* problem. This is a standard Least Squares (LS) problem whose solution is given by

$$\boldsymbol{\Theta}_{\rm LS} = \alpha\bar{\boldsymbol{\Theta}}_{\rm LS}, \tag{12}$$

$$\bar{\boldsymbol{\Theta}}_{\rm LS} \triangleq -(\boldsymbol{T}^T\boldsymbol{\Phi}_{\mathcal{B}}\boldsymbol{T})^{-1}(\boldsymbol{T}^T\boldsymbol{\Phi}_{\mathcal{B}}\boldsymbol{S}), \tag{13}$$

with $\bar{\boldsymbol{\Theta}}_{\rm LS}$ the LS solution for $\alpha = 1$. Then the transmit power required by the LS solution (12) can be written as

$$\begin{aligned} P_{\rm LS} &= \mathrm{tr}\{\boldsymbol{G}^H(\boldsymbol{\Theta}_{\rm LS})\boldsymbol{\Phi}_{\mathcal{T}}\boldsymbol{G}(\boldsymbol{\Theta}_{\rm LS})\} \\ &= \alpha^2\underbrace{\mathrm{tr}\{\boldsymbol{G}_1^H(\bar{\boldsymbol{\Theta}}_{\rm LS})\boldsymbol{\Phi}_{\mathcal{T}}\boldsymbol{G}_1(\bar{\boldsymbol{\Theta}}_{\rm LS})\}}_{\triangleq P_1}, \end{aligned} \tag{14}$$

where $\boldsymbol{G}_1(\boldsymbol{\Theta}) \triangleq \boldsymbol{S} + \boldsymbol{T}\boldsymbol{\Theta}$ corresponds to the operator $\boldsymbol{G}$ for $\alpha = 1$, and P_1 denotes the transmit power required by the LS solution when $\alpha = 1$. Then, if $P_{\rm LS} < P_{\max}$, it is clear that $\boldsymbol{\Theta}_{\rm LS}$ is the solution of the constrained problem (11). On the other hand, if $P_{\rm LS} \ge P_{\max}$, then the unconstrained optimum is not feasible, and at the solution of (11) the constraint must hold with equality. Note that, in view of (14), the condition $P_{\rm LS} \ge P_{\max}$ amounts to checking whether

$$\alpha^2 \ge \frac{P_{\max}}{P_1} \triangleq \alpha_\star^2. \tag{15}$$

Note that this threshold value $\alpha_\star^2$ only depends on system parameters (through matrices $\boldsymbol{S}$, $\boldsymbol{T}$, $\boldsymbol{\Phi}_\mathcal{T}$ and $\boldsymbol{\Phi}_\mathcal{B}$) and can be easily computed beforehand. When the chosen value of α satisfies (15), then one must solve an LS problem with a quadratic equality constraint $\mathrm{tr}\{\boldsymbol{G}^H(\boldsymbol{\Theta})\boldsymbol{\Phi}_\mathcal{T}\boldsymbol{G}(\boldsymbol{\Theta})\} = P_{\text{max}}$, which can be done by means of Lagrange multipliers.

In order to proceed, we first rewrite (11) to show the dependence on the optimization variables. Partition $\boldsymbol{\Theta}$ and $\boldsymbol{S}$ columnwise as

$$\boldsymbol{\Theta} = [\ \boldsymbol{\theta}_1\ \ \boldsymbol{\theta}_2\ \ \cdots\ \ \boldsymbol{\theta}_{N_D}\ ], \qquad \boldsymbol{S} = [\ \boldsymbol{s}_1\ \ \boldsymbol{s}_2\ \ \cdots\ \ \boldsymbol{s}_{N_D}\ ], \tag{16}$$

and then, since $\boldsymbol{G}(\boldsymbol{\Theta}) = \alpha\boldsymbol{S} + \boldsymbol{T}\boldsymbol{\Theta}$, note that for any $N \times N$ matrix $\boldsymbol{M}$ one has

$$\begin{aligned}\mathrm{tr}\{\boldsymbol{G}^H\boldsymbol{M}\boldsymbol{G}\} &= \alpha^2\,\mathrm{tr}\{\boldsymbol{S}^T\boldsymbol{M}\boldsymbol{S}\} + \mathrm{tr}\{\boldsymbol{\Theta}^H\boldsymbol{T}^T\boldsymbol{M}\boldsymbol{T}\boldsymbol{\Theta}\} \\ &\quad + 2\alpha\,\mathrm{tr}\{\Re\{\boldsymbol{\Theta}^H\boldsymbol{T}^T\boldsymbol{M}\boldsymbol{S}\}\} \qquad (17)\\ &= \alpha^2\,\mathrm{tr}\{\boldsymbol{S}^T\boldsymbol{M}\boldsymbol{S}\} + \sum_{i=1}^{N_D}\boldsymbol{\theta}_i^H\boldsymbol{T}^T\boldsymbol{M}\boldsymbol{T}\boldsymbol{\theta}_i \\ &\quad + 2\alpha\sum_{i=1}^{N_D}\Re\{\boldsymbol{\theta}_i^H\boldsymbol{T}^T\boldsymbol{M}\boldsymbol{s}_i\}. \qquad (18)\end{aligned}$$

Denote now the contribution of the data subcarriers to the total power and to the power leaked over band $\mathcal{B}$ respectively by

$$P_{d_\mathcal{T}} = \alpha^2\,\mathrm{tr}\{\boldsymbol{S}^T\boldsymbol{\Phi}_\mathcal{T}\boldsymbol{S}\}, \qquad P_{d_\mathcal{B}} = \alpha^2\,\mathrm{tr}\{\boldsymbol{S}^T\boldsymbol{\Phi}_\mathcal{B}\boldsymbol{S}\}. \tag{19}$$

In view of (18) and (19), we can rewrite the optimization problem (11) (with equality constraint) as

$$\begin{aligned}\min_{\{\boldsymbol{\theta}_i\}}\quad & P_{d_\mathcal{B}} + \sum_{i=1}^{N_D}\left[\boldsymbol{\theta}_i^H\boldsymbol{T}^T\boldsymbol{\Phi}_\mathcal{B}\boldsymbol{T}\boldsymbol{\theta}_i + 2\alpha\Re\left\{\boldsymbol{\theta}_i^H\boldsymbol{T}^T\boldsymbol{\Phi}_\mathcal{B}\boldsymbol{s}_i\right\}\right] \\ \text{s.t.}\quad & P_{d_\mathcal{T}} + \sum_{i=1}^{N_D}\left[\boldsymbol{\theta}_i^H\boldsymbol{T}^T\boldsymbol{\Phi}_\mathcal{T}\boldsymbol{T}\boldsymbol{\theta}_i + 2\alpha\Re\left\{\boldsymbol{\theta}_i^H\boldsymbol{T}^T\boldsymbol{\Phi}_\mathcal{T}\boldsymbol{s}_i\right\}\right] \\ & = P_{\text{max}}. \qquad (20)\end{aligned}$$

Consider now the eigendecompositions of the Hermitian matrices $\boldsymbol{T}^T\boldsymbol{\Phi}_\mathcal{B}\boldsymbol{T}$ and $\boldsymbol{T}^T\boldsymbol{\Phi}_\mathcal{T}\boldsymbol{T}$ featuring in (20):

$$\boldsymbol{T}^T\boldsymbol{\Phi}_\mathcal{B}\boldsymbol{T} = \boldsymbol{P}_A^H\boldsymbol{\Lambda}_A\boldsymbol{P}_A, \qquad \boldsymbol{T}^T\boldsymbol{\Phi}_\mathcal{T}\boldsymbol{T} = \boldsymbol{P}_B^H\boldsymbol{\Lambda}_B\boldsymbol{P}_B. \tag{21}$$

From (21), let us introduce the following matrices and vectors:

$$\boldsymbol{A} = \boldsymbol{P}_A^H\boldsymbol{\Lambda}_A^{1/2}\boldsymbol{P}_A, \qquad \boldsymbol{p}_i = \boldsymbol{A}^{-1}\boldsymbol{T}^T\boldsymbol{\Phi}_\mathcal{B}\boldsymbol{s}_i, \tag{22}$$

$$\boldsymbol{B} = \boldsymbol{P}_B^H\boldsymbol{\Lambda}_B^{1/2}\boldsymbol{P}_B, \qquad \boldsymbol{q}_i = \boldsymbol{B}^{-1}\boldsymbol{T}^T\boldsymbol{\Phi}_\mathcal{T}\boldsymbol{s}_i, \tag{23}$$

so that (20) becomes

$$\begin{aligned}\min_{\{\boldsymbol{\theta}_i\}}\ & P_{d_\mathcal{B}} + \sum_{i=1}^{N_D}\left[\boldsymbol{\theta}_i^H\boldsymbol{A}^H\boldsymbol{A}\boldsymbol{\theta}_i + 2\alpha\Re\left\{\boldsymbol{\theta}_i^H\boldsymbol{A}^H\boldsymbol{p}_i\right\}\right] \\ \text{s.t.}\ & P_{d_\mathcal{T}} + \sum_{i=1}^{N_D}\left[\boldsymbol{\theta}_i^H\boldsymbol{B}^H\boldsymbol{B}\boldsymbol{\theta}_i + 2\alpha\Re\left\{\boldsymbol{\theta}_i^H\boldsymbol{B}^H\boldsymbol{q}_i\right\}\right] = P_{\text{max}}.\end{aligned} \tag{24}$$

Equating to zero the gradient of the corresponding Lagrangian w.r.t. $\boldsymbol{\theta}_j$, it is seen that at the optimum value of the parameters the following conditions must hold for $1 \le j \le N_D$ (together with the constraint in (24)):

$$\boldsymbol{A}^H\boldsymbol{A}\boldsymbol{\theta}_j + \alpha\boldsymbol{A}^H\boldsymbol{p}_j + \lambda(\boldsymbol{B}^H\boldsymbol{B}\boldsymbol{\theta}_j + \alpha\boldsymbol{B}^H\boldsymbol{q}_j) = 0, \tag{25}$$

where λ is the Lagrange multiplier. The solution can be efficiently found by resorting to the Generalized Singular Value Decomposition (GSVD) [18, Ch. 12] of $\boldsymbol{A}$ and $\boldsymbol{B}$:

$$\boldsymbol{A} = \boldsymbol{U}\boldsymbol{D}_A\boldsymbol{X}^{-1}, \qquad \boldsymbol{B} = \boldsymbol{V}\boldsymbol{D}_B\boldsymbol{X}^{-1}, \tag{26}$$

where $\boldsymbol{U}$, $\boldsymbol{V}$ are unitary, $\boldsymbol{X}$ is invertible, and $\boldsymbol{D}_A$, $\boldsymbol{D}_B$ are diagonal and positive semidefinite with $\boldsymbol{D}_A^2 + \boldsymbol{D}_B^2 = \boldsymbol{I}$. Using (26), the solution to (25) is found to be

$$\boldsymbol{\theta}_j = -\alpha\boldsymbol{X}(\boldsymbol{D}_A^2 + \lambda\boldsymbol{D}_B^2)^{-1}(\boldsymbol{D}_A\boldsymbol{U}^H\boldsymbol{p}_j + \lambda\boldsymbol{D}_B\boldsymbol{V}^H\boldsymbol{q}_j), \tag{27}$$

for $j = 1, \ldots, N_D$. The value of the Lagrange multiplier must be obtained by substituting (27) in the expression of the power constraint in (24) and solving for λ in the resulting equation. Although such equation is nonlinear, its structure allows for efficiently finding a numerical solution, as shown in [18].

B. Selecting the set of cancellation subcarriers

The optimization of cancellation weights presented in Sec. III-A is based on fixed matrices $\boldsymbol{S}$ and $\boldsymbol{T}$, or equivalently, computed for a given allocation of the AIC subcarriers. We turn now to the problem of how to determine such allocation in order to obtain the best performance in terms of OBR reduction.

Since the protected band $\mathcal{B}$ spans N_P subcarriers which will never correspond to data subcarriers, the problem amounts to finding the optimal locations of the remaining N_C cancellation subcarriers. Therefore, the number of possible assignments is

$$\begin{pmatrix} N - N_P \\ N_C \end{pmatrix} = \frac{(N - N_P)!}{N_C!(N - N_P - N_C)!}, \tag{28}$$

which precludes an exhaustive search in view of the high values of N envisioned, even taking into account that such search can be performed offline ($N \ge 1024$) [14], [15].

Previous AIC schemes invariantly place half of the N_C cancellation subcarriers at the lower edge of the protected band $\mathcal{B}$ and the other half at the upper edge. The rationale for this choice is likely to be the impression that, since the spectrum (3) of each individual subcarrier falls off as one departs from its central frequency, packing the available AIC subcarriers as close as possible to the protected band should have the largest effect in terms of OBR.

We argue that this is not necessarily the case. In order to illustrate this effect, consider the simplest case in which the N_P subcarriers overlapping the protected band are simply turned off, and there is a single AIC subcarrier left ($N_C = 1$). Assume that $\alpha^2 \le \alpha_\star^2$, so that the unconstrained LS solution (12)–(13) is optimal. It is straightforward to check that the OBR obtained in this way is given by

$$\begin{aligned}\int_\mathcal{B} P_x(f)\mathrm{d}f &= \mathrm{tr}\{\boldsymbol{G}^H(\boldsymbol{\Theta}_{\text{LS}})\boldsymbol{\Phi}_\mathcal{B}\boldsymbol{G}(\boldsymbol{\Theta}_{\text{LS}})\} \\ &= \alpha^2\left[\mathrm{tr}\{\boldsymbol{\Phi}_\mathcal{B}\} - \frac{\sum_j\left|\int_\mathcal{B}\phi_k(f)\phi_j(f)\mathrm{d}f\right|^2}{\int_\mathcal{B}|\phi_k(f)|^2\mathrm{d}f}\right], \qquad (29)\end{aligned}$$

where k is the index of the AIC subcarrier, and the summation runs over all indexes j corresponding to subcarriers not in $\mathcal{B}$. Thus, finding the optimal position of the AIC subcarrier amounts to minimizing (29) with respect to k. In order to

illustrate the behavior of (29) in terms of the AIC subcarrier index k, note that *both* the numerator and the denominator of the quotient within brackets in (29) become smaller as k moves away from the protected band $\mathcal{B}$, although since the integrals in the numerator appear squared, one could expect the numerator to decay faster. Thus, eventually as k departs from $\mathcal{B}$, the OBR (29) should start to increase. However, this does not imply that (29) is monotonically increasing with k, and in fact the smallest OBR value need not take place at the edge of $\mathcal{B}$. Fig. 1 shows the OBR values obtained in a setting with $N = 1024$, $N_{\text{cp}} = 48$ and $N_P = 20$, with $N_C = 1$ cancellation subcarrier and $\alpha^2 = 0.99$. Observe that the OBR obtained by the unconstrained LS solution behaves in a quasiperiodic manner in terms of the AIC subcarrier separation from the band edge. But it is seen that the unconstrained solution turns out to violate the power constraint for separations larger than three subcarriers. If one looks at the behavior of the *constrained* solution, two observations can be made: first, for large separations the OBR tends to increase, as expected. Second, the smallest OBR value *does not* take place at the smallest separation (in this example it takes place for a separation of ten subcarriers).

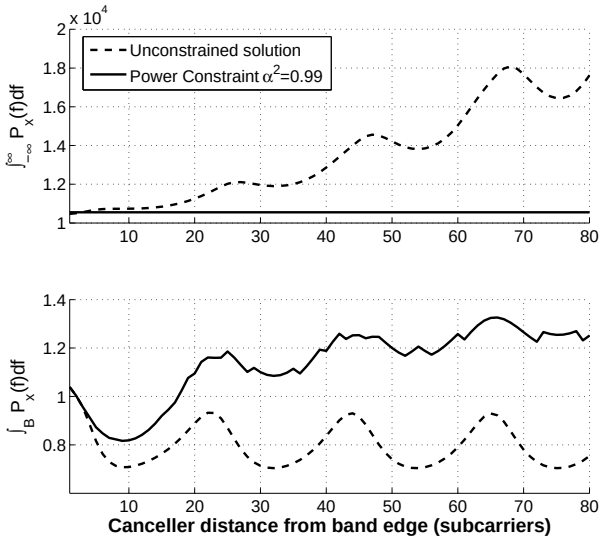

Fig. 1. Total transmit power (top) and OBR (bottom) of the unconstrained and constrained solutions with a single AIC subcarrier ($N_C = 1$) in terms of its separation from the band edge. $N = 1024$, $N_{\text{cp}} = 48$, $N_P = 20$.

In view of these considerations, it seems sensible to limit the search for the optimum positions of the N_C AIC subcarriers to the $\bar{N}$ positions right below (resp. above) the protected band's lower (resp. upper) edge. The choice of $\bar{N}$ should trade off complexity and performance, since the number of candidate assignments becomes

$$\binom{\bar{N}}{N_C} = \frac{\bar{N}!}{N_C!(\bar{N} - N_C)!}. \tag{30}$$

While this *proximity narrowing* of the search set represents a huge reduction with respect to (28) for realistic values of N, it is still a very large set to be practical, as illustrated by the numerical example in Table I.

The search set can be further reduced due to the symmetry of the problem. Consider the contribution of the data subcarriers to the OBR given in (19):

$$P_{d_{\mathcal{B}}} = \alpha^2 \,\text{tr}\{\boldsymbol{S}^T \boldsymbol{\Phi}_{\mathcal{B}} \boldsymbol{S}\} = \alpha^2 \sum_{k \in \mathcal{D}} \int_{\mathcal{B}} |\phi_k(f)|^2 \text{d}f, \tag{31}$$

where $\mathcal{D}$ denotes the set of indexes of the data subcarriers. Since the functions $\phi_k(f)$ are shifted replicas of the same symmetric and periodic (with period M) function, then the OBR introduced by those data subcarriers at the left of the protected band $\mathcal{B}$ is equal to that introduced by the data subcarriers at its right. Therefore, it is reasonable to assume that if an AIC subcarrier placed Q positions below $\mathcal{B}$'s lower edge results optimal, then a cancellation subcarrier chosen Q positions above $\mathcal{B}$'s upper edge will also result optimal. Therefore, the search can be narrowed to $\bar{N}/2$ subcarriers at one side of the protected band, assuming symmetric locations for the cancellation subcarriers on the other side. In this way, the number of candidate assignments becomes

$$\binom{\bar{N}/2}{N_C/2} = \frac{\bar{N}/2!}{N_C/2!(\bar{N}/2 - N_C/2)!}. \tag{32}$$

Unfortunately, as shown in the example in Table I, the search set resulting from this *symmetry narrowing* can still be too large for practical implementation. To overcome this problem, a suboptimal greedy scheme is proposed next in order to further reduce the set of candidate assignments. This greedy search is detailed in Algorithm 1 and is based on adding one new pair of symmetrically placed cancellation subcarriers at each step, selecting the new pair as the one that provides the greatest performance improvement from the previous step. The algorithm is initialized by defining the set of cancellation subcarriers as including only the N_P subcarriers aligned with the protected band $\mathcal{B}$, over which data transmission is always precluded. Then the algorithm iterates $N_C/2$ times to determine the remaining cancellation subcarrier positions. At each iteration, the OBR improvement attained with the addition of each possible pair of symmetrically positioned (with respect to band $\mathcal{B}$) subcarriers to the set of cancelers is computed as described in Sec. III-A. Then, the pair of subcarriers obtaining the largest OBR reduction is added to the set of cancelers and removed from the set of data subcarriers before the next iteration. Though not necessarily optimal, extensive simulation results show that the output of this greedy scheme is very close to the optimal solution obtained by exhaustive search over the number of candidate assignments given by (32), and with much fewer steps (less than $N_C \times \bar{N}$).

We have observed that the result of the greedy search can be often improved further with a final refinement stage. In such stage, we perturb each symmetric pair of the AIC subcarriers obtained by the greedy approach by a few positions (as long as those positions are not already occupied by another pair of AIC subcarriers) and evaluate the optimum OBR attainable with the perturbed locations, retaining the best of all those settings. In the results presented in Sec. V using realistic system parameters, considering perturbations of just one subcarrier index in the refinement stage was enough to find the globally

Algorithm 1 Greedy search for AIC subcarrier allocation.

Definition: *PU band* $\mathcal{B}$
  Subcarriers aligned with $\mathcal{B} \rightarrow k \in \{m_1, \ldots, m_{N_P}\}$
  with $m_n = m_1 + (n-1)$, $n = 1, \ldots, N_P$
Initialization:
  AIC Subcarriers: $\mathcal{C} = \{k : k \in \{m_1, \ldots, m_{N_P}\}\}$
  Search Set: $\mathcal{S} = \{k : k \in \{1, \ldots, \bar{N}/2\}\}$
  for Cancel $= 1$ to $N_C/2$ **do**
    OBR $= \infty$
    for $k \in \mathcal{S}$ **do**
      $\mathcal{C}^* = \mathcal{C} \cup \{m_1 - k, m_{N_P} + k\}$
      Compute the optimum $\boldsymbol{G}$ based on $\mathcal{C}^*$
      trial_value $= \mathrm{tr}\{\boldsymbol{G}^H \boldsymbol{\Phi}_{\mathcal{B}} \boldsymbol{G}\}$
      if trial_value $<$ OBR **then**
        OBR $=$ trial_value
        $k^* = k$
      end if
    end for
    $\mathcal{C} = \mathcal{C} \cup \{m_1 - k^*, m_{N_P} + k^*\}$
    Remove k^* from $\mathcal{S}$
  end for

optimal result. This final refinement search is performed over at most $(3/2N_C)!/((N_C/2)!N_C!)$ candidate assignments.

IV. Complexity Analysis

We split the complexity analysis of the PU protection scheme derived in Sec. III, termed *PSD-AIC*, in two parts: online complexity (computation of the cancellation coefficients $\boldsymbol{c}$ as per (5)), and offline complexity (related to the search for the optimal location of the AIC subcarriers).

A. Online computational cost

Disregarding the effect of matrices $\boldsymbol{S}$ and $\boldsymbol{T}$, which just map cancellation coefficients and data symbols to subcarriers, the online complexity for *PSD-AIC* is given by the computation of (5), which requires only $2 \times (N_C + N_P) \times N_D$ operations. This small online cost is achieved because most of the computational effort, i.e. the optimization of the cancellation weights $\boldsymbol{\Theta}$, is performed offline.

This is not the case in previous solutions [4],[6]. Specifically, the online computational cost of previous AIC schemes strongly depends on the frequency resolution, that is, the number of frequency points in band $\mathcal{B}$ considered in the optimization. In the proposed *PSD-AIC* approach, although the integration step required in order to compute the matrices $\boldsymbol{\Phi}_{\mathcal{B}}$ and $\boldsymbol{\Phi}_{\mathcal{T}}$ in (10) has to be carried out numerically in general, and this step also involves choosing the frequency resolution, this has no impact on the online complexity, so this resolution can be chosen as high as desired. As will be shown in Sec. V, the proposed *PSD-AIC* approach leads to improved PU protection performance thanks to the better spectral resolution available.

B. Assignment optimization cost

The search for the best set of AIC subcarriers requires the computation of the optimal *PSD-AIC* weights (which is done by solving either an unconstrained LS or a quadratically constrained LS problem) for a number of candidate assignments. The last column of Table II summarizes the number of required optimization steps for the different assignment selection procedures discussed in Sec. III-B. A numerical example using practical values of system parameters is given in Table I, in order to better illustrate the complexity savings involved. As seen in Table I, whereas an exhaustive search for the globally optimum assignment results computationally intensive, and very likely unfeasible, assignment optimization becomes practical by resorting to the proposed heuristics, and especially the proposed greedy search. Again, note that the effort invested in the AIC assignment optimization does not affect the online complexity of the resulting scheme.

TABLE I
Numerical example of the computational cost of the assignment schemes. $N = 1024$, $N_C = 8$, $N_P = 20$, $\bar{N} = 40$

	Search set size	Steps required
Proximity narrowing	$\approx 77 \cdot 10^6$	$\approx 77 \cdot 10^6$
Symmetry narrowing	$4,845$	$4,845$
Greedy search	$4,845$	74
Greedy+refinement	$4,845$	$300 - 600$

TABLE II
Computational cost of the AIC subcarrier assignment schemes

	Search set size	No. of steps required
Full search	$\frac{(N-N_P)!}{N_C!(N-N_P-N_C)!}$	$\frac{(N-N_P)!}{N_C!(N-N_P-N_C)!}$
Proximity narrowing	$\frac{\bar{N}!}{N_C!(\bar{N}-N_C)!}$	$\frac{\bar{N}!}{N_C!(\bar{N}-N_C)!}$
Symmetry narrowing	$\frac{(\bar{N}/2)!}{(N_C/2)!(N/2-N_C/2)!}$	$\frac{(\bar{N}/2)!}{(N_C/2)!(N/2-N_C/2)!}$
Greedy search	$\frac{(\bar{N}/2)!}{(N_C/2)!(N/2-N_C/2)!}$	$< N_C\bar{N}$
Greedy+refinement	$\frac{(\bar{N}/2)!}{(N_C/2)!(N/2-N_C/2)!}$	$< N_C\bar{N} + \frac{3N_C/2!}{N_C/2!N_C!}$

V. *PSD-AIC* PU protection performance

In this section we evaluate the performance of the proposed *PSD-AIC* design, which optimizes both the AIC subcarrier assignment and the corresponding weights. In order to ease the comparison with previous AIC designs, which do not consider the optimization of the AIC subcarrier locations, *PSD-AIC* is first evaluated for a fixed AIC subcarrier assignment. Then, the performance gain obtained by assignment optimization is addressed from those baseline results.

In order to obtain a realistic evaluation, OFDM system parameters are chosen based on current standards specifications [14], [15]. We consider a cognitive OFDM system consisting of $N = 1024$ subcarriers, together with a narrowband PU lying within the SU spectrum and with a bandwidth equivalent to $N_P = 20$ subcarriers. Data symbols to be modulated on the data subcarriers are i.i.d. and chosen from a $16-$QAM constellation. A $3/64$ CP (5%) is used, equivalent to 48 samples. Transmission power is shared between data and cancellation subcarriers through parameter α (see (6)), which

TABLE III

MEAN NOTCH DEPTH OVER $\mathcal{B}$ FOR STANDARD ASSIGNMENT

	$N_C = 6$	$N_C = 8$	$N_C = 10$
Full load	-17.8	-17.8	-17.8
Null subcarriers	-20.6	-21.1	-21.6
PSD-AIC $\alpha^2 = 0.99$	-28.1	-31.9	-36.8
PSD-AIC $\alpha^2 = 0.98$	-30.2	-36.2	-40.3
PSD-AIC $\alpha^2 = 0.97$	-32.0	-38.6	-41.8
PSD-AIC $\alpha^2 = 0.96$	-33.6	-39.9	-42.5
PSD-AIC $\alpha^2 = 0.95$	-34.9	-40.7	-43.1

Mean notch depth is expressed in dB. $N = 1024$, $N_P = 20$.

is varied from $\alpha^2 = 0.99$ to $\alpha^2 = 0.95$ such that the power spent on the cancellation subcarriers is a small fraction of the available power.

A. Performance evaluation for a fixed assignment

In order to compare the proposed *PSD-AIC* design against previous OBR reduction schemes, we use the standard assignment in which all of the N_C cancellation subcarriers are placed at the edges of the protected PU band.

For such setting, the performance of *PSD-AIC* is summarized in Table III for different power splits between data and cancellation subcarriers and considering different numbers of cancellation subcarriers. The table also includes results for a fully loaded system which only turns off the N_P subcarriers aligned with the protected PU band, as well as for a system which turns off the $N_P + N_C$ reserved subcarriers. Note that simply turning off subcarriers is not an effective means to reduce OBR. In contrast, active interference cancellation achieves much deeper notches at the affordable price of a small power penalty. For example, for $N_C = 8$ and $\alpha^2 = 0.97$ the notch depth is increased about 17 dB and 21 dB with respect to the null subcarriers and the fully loaded cases, respectively.

Next we compare the proposed *PSD-AIC* design with the AIC schemes from [4] and [6], referred to in the sequel as *AIC* and *SR-AIC* respectively. Both *AIC* and *SR-AIC* are based on the minimization of the SU spectrum over a discrete set of frequencies within $\mathcal{B}$. We take $M_{\mathcal{B}} = 10$ samples per sidelobe, as suggested by the authors in order to keep online computational load reasonable (the cancellation coefficients are computed *online* for each OFDM symbol in both schemes). On the other hand, the matrices $\mathbf{\Phi}_{\mathcal{B}}$ and $\mathbf{\Phi}_{\mathcal{T}}$ featuring in the proposed method are evaluated numerically *offline* using a frequency resolution of 100 samples per sidelobe. Regarding the power constraint on the cancellation subcarriers, whereas *AIC* is designed under a power constraint equivalent to the one employed in this paper, this is not the case for *SR-AIC*, which sets *individual* power constraints for each cancellation subcarrier. In the results presented here, these constraints are set all equal.

Regarding uncoded bit error rate (BER), and assuming an AWGN channel, it is clear that all AIC schemes exhibit a fixed SNR loss due to the power allocated to the cancellation subcarriers. This SNR loss equals $10 \log_{10} \alpha^2$ dB, which for the values in Table III ranges between 0.04 and 0.22 dB.

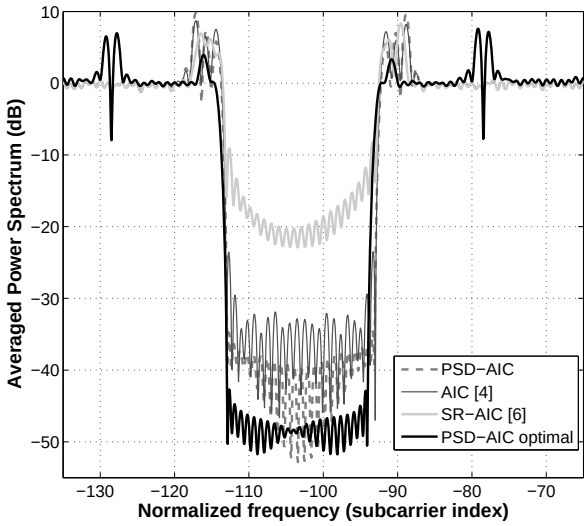

Fig. 2. Averaged power spectrum for *PSD-AIC*, *AIC* [4] and *SR-AIC* [6] for $N_C = 8$ and $\alpha^2 = 0.97$. Results are averaged over 500 OFDM symbols.

TABLE IV

ONLINE COMPUTATIONAL COST FOR COMPARED AIC SCHEMES.

	Online complexity	Example
PSD-AIC	$2(N_C + N_P)N_D$	$55,776$
AIC [4]	$\mathcal{O}(2NM_{\mathcal{B}} + 1/2N_C^2 M_{\mathcal{B}} + 2/3N_C^3) + 2M_{\mathcal{B}}(N_C + N_P)N_D$	$> 578,789$
SR-AIC [6]	$2NM_{\mathcal{B}} + 2M_{\mathcal{B}}(N_C + N_P)N_D$	$578,240$

Last column indicates approximate load for the parameters of Fig. 2.

Fig. 2 shows the power spectra obtained by the different designs using $N_C = 8$ cancellation subcarriers and $\alpha^2 = 0.97$. The main difference in performance between *SR-AIC* and both *AIC* and *PSD-AIC* arises for the different constraint used. The multiple power constraints used in *SR-AIC* are more restrictive on the cancellation coefficients, leading to a significant performance loss in terms of OBR reduction. On the other hand, performance of *AIC* and proposed *PSD-AIC* is comparable, although favoring the latter. In this case the power constraints in the two optimization problems are equivalent and the better performance of *PSD-AIC* is due to the finer frequency resolution, which is obtained without compromising online computational cost.

In order to emphasize the fact that the standard allocation of cancellation subcarriers provides a baseline for the performance of the proposed design, the results obtained after optimizing the locations of these subcarriers are also included in Fig. 2. A 7 dB performance gain is observed without affecting the online computational cost.

TABLE V
MEAN NOTCH DEPTH OVER $\mathcal{B}$ FOR OPTIMIZED ASSIGNMENT

	Standard	Greedy	Greedy+refinement
Full load	-17.8	–	–
Null subcarriers	-21.1	–	–
PSD-AIC $\alpha^2 = 0.99$	-31.9	-39.0	-42.7
PSD-AIC $\alpha^2 = 0.97$	-38.6	-45.6	-47.9
PSD-AIC $\alpha^2 = 0.95$	-40.7	-45.7	-48.0

Mean notch depth is expressed in dB. $N = 1024$, $N_P = 20$, $N_C = 8$.

The computational savings provided by the proposed scheme are illustrated in Table IV, where the online complexity for the three designs is shown. The impact of $M_{\mathcal{B}}$ (the number of samples per sidelobe for the set of discrete frequencies) becomes evident. The large complexity savings of *PSD-AIC* (more than 90% for the example shown in Fig. 2) come from the fact that its online computational cost is independent of the frequency resolution used. Note that although *SR-AIC* avoids the online gsvd operations required by *AIC*, their overall online complexities are similar for both schemes (and much higher than that of the proposed design). This happens because the online gsvd avoided by *SR-AIC* is of the order of N_C^3. When N is large, as in current standards [14][15], and assuming N_C is kept fixed, the number of frequency samples per subcarrier $M_{\mathcal{B}}$ becomes the limiting computational cost factor.

As seen in Fig. 2, one common feature of all AIC schemes is that all exhibit spectral peaks located around the positions of the cancellation subcarriers. The height of these peaks is directly related to the power allocated to the cancellation subcarriers. This could be a concern regarding the peak to average power ratio (PAPR) of the resulting waveform, which could result in performance losses after passage through a nonlinear amplifier. Fortunately, as will be shown later on in this section, for reasonable values of the power budget this loss is rather small.

B. Performance evaluation with optimized assignment

The impact of optimizing the location of cancellation subcarriers is analyzed next, in terms of both the power budget α^2 and the number of cancellation subcarriers N_C.

Table V shows the results obtained by the proposed design for $N_C = 8$ under different assignment types and power budgets. It is clear that by judiciously choosing the positions of the cancellation subcarriers yields a very significant improvement (in the range 7–10 dB in this example) with respect to the standard assignment, which in turn already provided much better performance than the baseline scheme that turns off the N_C subcarriers.

Also note that performing a local search (refinement) in the vicinity of the solution produced by the greedy method improves the performance in 2–3 dB. In this example, this local search was conducted within the set of positions immediately adjacent to the locations obtained by the greedy scheme; as a result, the global optimum was found (this was checked by performing a computationally intensive exhaustive search). Although there is no guarantee that this procedure will always find the globally optimum assignment in all possible scenarios, the performance of the (suboptimal) solutions produced is significantly better than that corresponding to standard assignments, and the cost incurred is manageable as illustrated in Table I.

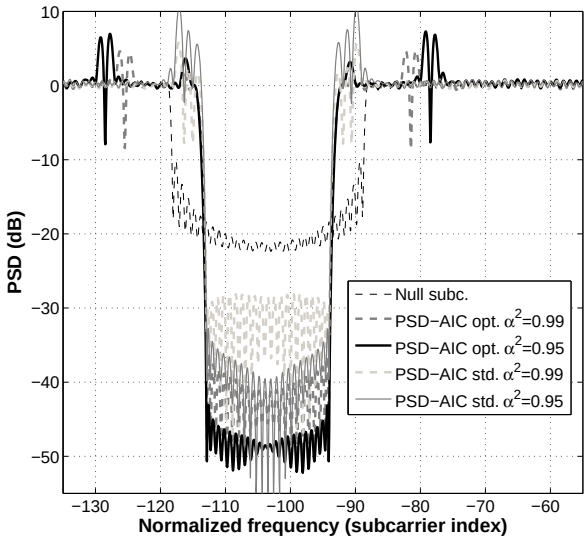

Fig. 3. PSDs of proposed *PSD-AIC* for $N_C = 10$ cancellation subcarriers and different values of α^2.

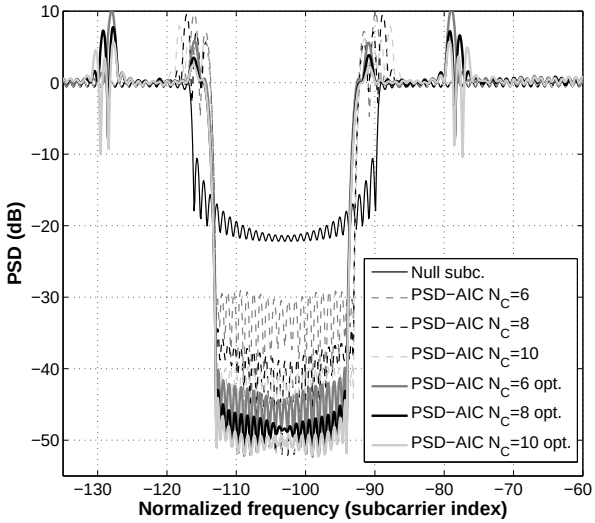

Fig. 4. PSDs of proposed *PSD-AIC* for $\alpha^2 = 0.97$ and different number of cancellation subcarriers.

It is also observed from Table V that with optimized subcarrier assignments the effect of allocating more power for cancellation becomes less pronounced than for the standard assignment. This effect can also be seen in Fig. 3, which shows the behavior of *PSD-AIC* with and without assignment optimization, fixing $N_C = 10$ subcarriers and for two different

values of α^2. This indicates that a much favorable tradeoff between SNR loss at the receiver and OBR reduction at the transmitter can be achieved.

In Fig. 4 we fix $\alpha^2 = 0.97$ and try different values of N_C. It is seen that the optimal locations are quite different from the standard ones: although a group of cancellation subcarriers is still placed at the edges of the protected band, there are some others clustered further away. This separation between cancellation subcarriers translates into lower spectrum peaks, as seen in both Figs. 3 and 4. Note also that increasing N_C for a given α improves the notch depth while shrinking the spectrum peaks, as cancellation power is distributed among a larger number of subcarriers. This is observed for both standard and optimized assignments.

C. Experimental validation

The proposed *PSD-AIC* scheme was implemented in two different hardware platforms to validate the design and its effectiveness in the face of circuitry-related impairments, by measuring the average power spectrum and comparing against the simulation results.

The following setup was used to generate the spectrally compensated OFDM signal. On one hand, a Rohde&Schwarz SMJ100A vector signal generator was employed to evaluate differences between simulation and measurement results. The precision provided by this high-end equipment makes it possible to validate the PSD approximation in (7) that was used to derive the weight optimization method of Sec. III-A. On the other hand, the OFDM signal was also synthesized by means of a Universal Software Radio Peripheral (USRP) platform [19], with the goal of evaluating the sensitivity of the proposed scheme to commercial hardware imperfections. The development kit for the transmission chain consists in this case of a personal computer to generate I/Q baseband samples, an USRP N210 motherboard and an SBX daughterboard. In both cases, average power spectrum was measured with a Rohde&Schwarz FSP30 spectrum analyzer.

As previously, OFDM system parameters were $N = 1024$, 16-QAM modulation and 3/64 cyclic prefix. The sampling rate is fixed to 2 MHz, with carrier frequency of 2.4 GHz. For the test using the Rhode&Schwarz generator, three different PU protected bands of different widths were placed within the SU passband, with $\mathcal{B}_1$ aligned with subcarriers 100 to 139 (40 subcarriers bandwidth), $\mathcal{B}_2$ aligned with subcarriers 400 to 419 (20 subcarriers bandwidth, as in Figs. 2–4), and $\mathcal{B}_3$ aligned with subcarriers 800 to 859 (60 subcarriers bandwidth). $N_C = 8$ cancellation subcarriers were used for each band, thus resulting in a total of 24 cancelers. As three protected bands are considered, the power allocated to the cancelers in these measurements is three times higher ($\alpha^2 = 0.91$) to get protection levels equivalent to those of Figs. 2 and 4 for which $\alpha^2 = 0.97$. Canceler locations are optimized separately for each protected band using the greedy+refinement approach; once these locations are fixed, cancellation weights are computed jointly for the three bands. Fig. 5 shows these results. Measured spectra indicate a good match with simulation results, as both notch depth and spectrum peak values are coincident, clearly validating the derivations presented in Sec. III-A. It is also worth noting that the notch depth obtained for the three protected bands is similar, due to the fact that the number of cancellation subcarriers and power allocated to them is the same. Fig. 6 zooms on the central PU band $\mathcal{B}_2$, to be compared with Figs. 2 and 4.

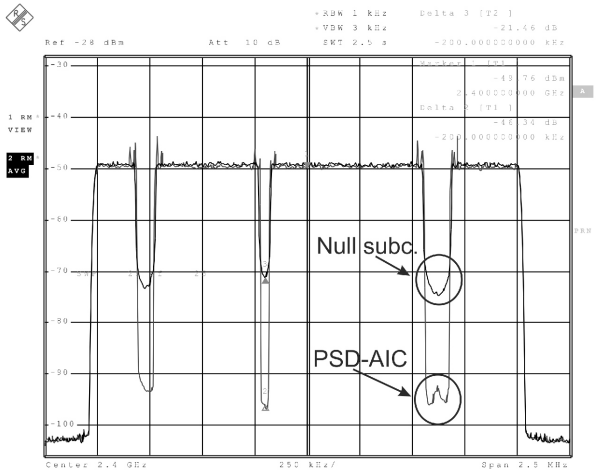

Fig. 5. Experimental measurement of average power spectra for signals synthesized by the SMJ100A vector signal generator.

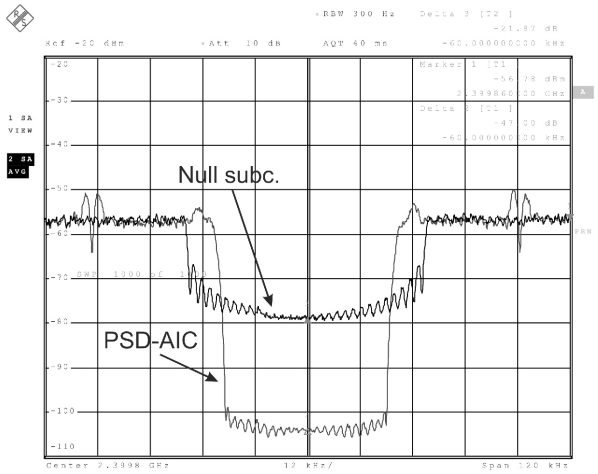

Fig. 6. Detail of measured average power spectra around protected band $\mathcal{B}_2$.

The results obtained by the implementation of *PSD-AIC* in the USRP hardware are presented next. This is an important measure of the applicability of the proposed scheme, since practical transceiver circuitry cannot be expected to meet the high quality of the SMJ100A. In particular, it has been observed that the USRP hardware cannot synthesize signals with a notch depth above 35 dB, suggesting that the deep notches shown in Fig. 5 may not be attained by commercial hardware platforms. However, on the USRP platform the proposed scheme still yields a significant improvement with narrower PU bands as shown in Fig. 7, in which a protected band with bandwidth corresponding to that of just five subcarriers is considered. Clearly the performance obtained by just turning off $N_C = 8$ subcarriers is unacceptable (less than 20 dB

attenuation). On the other hand, *PSD-AIC* produces a notch almost 35 dB deep with $N_C = 8$ and minimal power spent on the cancellation subcarriers ($\alpha^2 = 0.9995$). The result obtained using the Rhode&Schwarz generator is also included for reference.

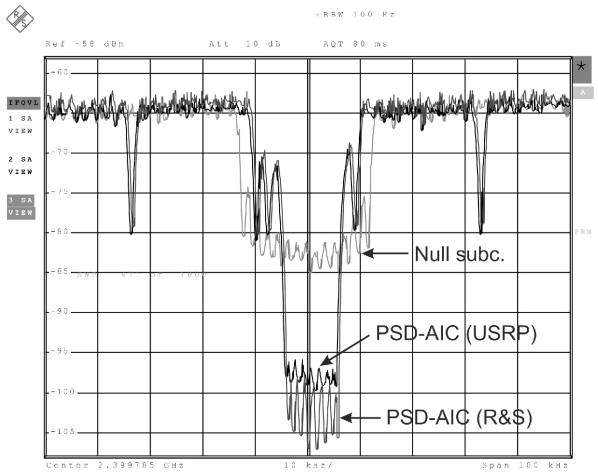

Fig. 7. Experimental measurement of average power spectra for PSD-AIC on USRP hardware platform. $N_C = 8$ and $\alpha^2 = 0.9995$.

As previously mentioned, one potential objection to AIC-based approaches is that spectrally compensated OFDM signals may exhibit larger PAPR values than those obtained by simply turning off subcarriers, which would translate in higher sensitivity to the nonlinear effects induced by power amplifiers (PAs). In order to test this, the signal generated by the SMJ100A whose spectrum is shown in Fig. 5 is downconverted to baseband, sampled at 100 Msamples/s, (optionally) digitally predistorted, upconverted to an Intermediate Frequency (IF) of 36.15 MHz in the digital domain and fed to a 100 Msamples/s digital-to-analog converter. Once back in the analog domain, the signal is upconverted to an UHF channel with 705.85 MHz carrier frequency and passed through a PA operating in its nonlinear region. The resulting signal is attenuated and fed to a Rohde&Schwarz ETL spectrum analyzer, with results shown in Fig. 8. Comparing Figs. 5 and 8, it is observed that (i) as a result of the processing steps just described, the noise floor has raised about 15 dB; (ii) the depth of the spectrum notches has decreased accordingly; (iii) the digital predistorter mitigates the performance loss over the protected band, in a similar amount as the spectral regrowth outside the system bandwidth is reduced. This suggests that digital predistortion, commonly used to reduce adjacent channel interference induced by spectral regrowth, is also effective at mitigating the performance loss of AIC-based schemes due to the PA-induced in-band interference.

VI. Conclusions

A novel Active Interference Cancellation design has been presented for primary user protection in cognitive OFDM systems. It was shown that the optimization of cancellation weights based on the power spectral density results in low online complexity of the proposed scheme, since most of the computational load corresponds to the offline design. Further, the proposed approach also allows optimizing the locations of the cancellation subcarriers, for which an efficient greedy algorithm has been proposed in order to deal with the combinatorial nature of the optimization problem. This results in significant improvements with respect to the standard approach, which places all cancellation subcarriers at the edges of the protected band, and without involving any additional tradeoff. Analogously to other AIC schemes, our design does not require transmission of side information and is completely transparent for operation of the receiver. Simulations and tests with diverse hardware platforms have shown that the proposed scheme is able to outperform previous AIC-based methods in terms of primary user protection at a much lower computational cost, obtaining notch depths of almost 50 dB in typical settings.

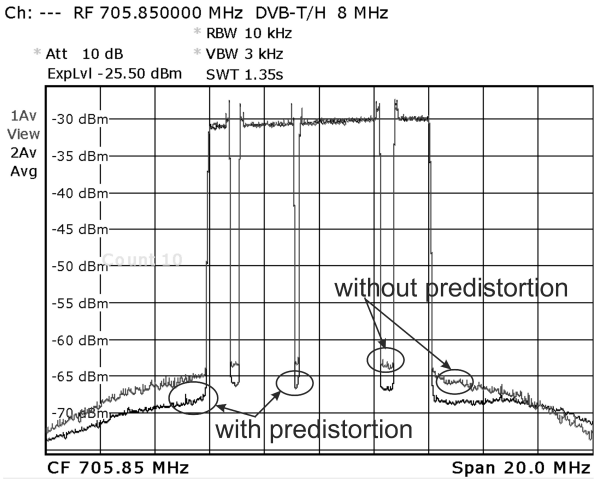

Fig. 8. Power spectra at the output of the PA, with and without digital predistortion.

References

[1] M. Bellanger, "Physical layer for future broadband radio systems," in *IEEE Radio and Wireless Symposium (RWS)*, 2010, pp. 436–439.

[2] I. Cosovic and V. Janardhanam, "Sidelobe suppression in OFDM systems," in *MCSS*, 2005, pp. 473–482.

[3] S. Pagadarai, R. Rajbanshi, A. Wyglinski, and G. Minden, "Sidelobe suppression for OFDM-based cognitive radios using constellation expansion," in *IEEE Wireless Comm. and Networking Conf. (WCNC)*, Apr. 2008, pp. 888–893.

[4] S. Brandes, I. Cosovic, and M. Schnell, "Reduction of out-of-band radiation in OFDM systems by insertion of cancellation carriers," *IEEE Comm. Letters*, vol. 10, no. 6, pp. 420–422, Jun. 2006.

[5] H. Yamaguchi, "Active interference cancellation technique for MB-OFDM cognitive radio," in *34th European Microwave Conf.*, vol. 2, Oct. 2004, pp. 1105–1108.

[6] S.-G. Huang and C.-H. Hwang, "Improvement of active interference cancellation: avoidance technique for OFDM cognitive radio," *IEEE Trans. on Wireless Comm.*, vol. 8, no. 12, pp. 5928–5937, Dec. 2009.

[7] D. Qu, Z. Wang, and T. Jiang, "Extended active interference cancellation for sidelobe suppression in cognitive radio OFDM systems with cyclic prefix," *IEEE Trans. on Vehicular Technology*, vol. 59, no. 4, pp. 1689–1695, May 2010.

[8] A. Batra, S. Lingam, and J. Balakrishnan, "Multi-band OFDM: a cognitive radio for UWB," in *IEEE Int. Symp. on Circuits and Systems (ISCAS)*, May 2006.

[9] J. Zhang, X. Huang, A. Cantoni, and Y. Guo, "Sidelobe suppression with orthogonal projection for multicarrier systems," *IEEE Trans. on Comm.*, vol. 60, no. 2, pp. 589–599, Feb. 2012.

[10] J. Van De Beek, "Sculpting the multicarrier spectrum: a novel projection precoder," *IEEE Comm. Letters*, vol. 13, no. 12, pp. 881–883, Dec. 2009.
[11] H.-M. Chen, W.-C. Chen, and C.-D. Chung, "Spectrally precoded OFDM and OFDMA with cyclic prefix and unconstrained guard ratios," *IEEE Trans. on Wireless Comm.*, vol. 10, no. 5, pp. 1416–1427, May 2011.
[12] M. Ma, X. Huang, B. Jiao, and Y. Guo, "Optimal orthogonal precoding for power leakage suppression in DFT-based systems," *IEEE Trans. on Communications*, vol. 59, no. 3, pp. 844–853, Mar. 2011.
[13] R. Xu and M. Chen, "A precoding scheme for DFT-based OFDM to suppress sidelobes," *IEEE Comm. Letters*, vol. 13, no. 10, pp. 776–778, Oct. 2009.
[14] 3GPP, "Physical layer aspects for evolved UTRA," 3GPP technical report, TR 25.814, Ver. 7.1.0, 2009.
[15] WiMax, "IEEE standard for local and metropolitan area networks part 16: Air interface for fixed and mobile broadband wireless access systems," IEEE Std 802.16e, 2006.
[16] T. Magesacher, "Spectral compensation for multicarrier communication," *IEEE Trans. Signal Process.*, vol. 55, no. 7, pp. 3366–3379, Jul. 2007.
[17] T. van Waterschoot, V. Le Nir, J. Duplicy, and M. Moonen, "Analytical expressions for the power spectral density of CP-OFDM and ZP-OFDM signals," *IEEE Signal Proc. Letters*, vol. 17, no. 4, pp. 371–374, Apr. 2010.
[18] G. H. Golub and C. F. Van Loan, *Matrix Computations*, 3rd ed. The Johns Hopkins University Press, Oct. 1996.
[19] Ettus Research, "USRP family of products," 2013. [Online]. Available: http://ettus.com/

Jorge F. Schmidt (S06M10) received the B.Sc. and D.Sc. degrees in Electrical Engineering from the Universidad Nacional del Sur (UNS), Baha Blanca, Argentina, in 2005 and 2011, respectively. He is currently a Postdoctoral Fellow in the Signal Theory and Communications Department, Universidad de Vigo, Vigo, Spain.

His research interests are in the areas of adaptive signal processing and statistical signal processing for multiuser communication systems.

Secundino Costas-Sanz received the M.S. degree in telecommunications engineering and the M.S in signal processing from the University of Vigo, Vigo, Spain, in 2008 and 2011, respectively, where he is currently working. Since 2008, he has been with the Signal Processing in Communications Group, part of the Signal Theory and Communications Department, University of Vigo.

His research interests include signal processing, cognitive radio and digital communications.

Roberto López-Valcarce (S'95-M'01) received the Telecommunication Engineering degree from the University of Vigo, Vigo, Spain, in 1995, and the M.S. and Ph.D. degrees in electrical engineering from the University of Iowa, Iowa City, in 1998 and 2000, respectively. During 1995, he was a Project Engineer with Intelsis. He was a Postdoctoral Fellow of the Spanish Ministry of Science and Technology from 2001 to 2006. During that period, he was with the Signal Theory and Communications Department, Universidad de Vigo, where he is currently an Associate Professor. His main research interests lie in the area of adaptive signal processing, digital communications, and sensor networks. He holds two European patents in the field of adaptive processing applied to communications systems.

Dr. López-Valcarce was a recipient of a 2005 Best Paper Award of the IEEE Signal Processing Society. He served as an Associate Editor of the IEEE TRANSACTIONS ON SIGNAL PROCESSING from 2008 to 2011 and currently serves as a member of the IEEE Signal Processing for Communications and Networking Technical Committee.